Optics Letters

30-GBaud DP 16-QAM transmission in the E-band enabled by bismuth-doped fiber amplifiers

Aleksandr Donodin,[1,*] Mingming Tan,[1] Pratim Hazarika,[1] Vladislav Dvoyrin,[1] Ian Phillips,[1] Paul Harper,[1] Sergei K. Turitsyn,[1] and Wladek Forysiak[1]

[1]Aston Institute of Photonic Technologies, Aston University, Birmingham, B4 7ET, UK
*Corresponding author: a.donodin@aston.ac.uk

Received 24 June 2022; revised 24 August 2022; accepted 24 August 2022; posted 25 August 2022; published 28 September 2022

We report the transmission of five 30-GBaud dual polarization 16-QAM signals over 160 km of standard single-mode fiber in the E-band (1410–1460 nm). The transmission line consists of two 80-km spans and three independent bismuth-doped fiber amplifiers. The developed amplifiers feature a maximum gain of 27.3 dB, 33.8 dB, and 28.3 dB with a minimum noise figure of 4.8 dB, 4.7 dB, and 5.3 dB, respectively. The maximum signal Q^2 factor penalty is 4.5 dB, and the overall performance of the system is above the pre-forward-error-correction (FEC) threshold for a 10^{-15} post-FEC bit error rate. To the best of our knowledge, this is the record experimentally demonstrated transmission length for a coherent detection signal in the E-band.

https://doi.org/10.1364/OL.468796

Introduction. The ever growing demand for higher data traffic [1] is leading to novel research approaches to increase the capacity of dense wavelength division-multiplexed optical communication systems. The conventional optical networks exploit only 10 THz allowed by commercially available Er-doped fiber amplifiers in the C- and L-optical bands (1530–1620 nm). There are three main approaches to increase the capacity of fiber-optical transmission systems by the development of: higher-order modulation formats; spatial division multiplexing (SDM); and multi-band transmission (MBT) [2]. The most practical technique is arguably MBT capable to utilize the huge and still available spectral bandwidth of the existing fiber base. Unlike SDM, MBT does not require a new fiber deployment. Moreover, the capacity of MBT scales linearly with a spectral bandwidth comparable to that of the higher-order modulation formats scaling logarithmically with the signal-to-noise ratio (SNR) [3]. Thus, the MBT maximizes the return-on-investment in the existing infrastructures [2] by the transmission in the so-called O, E, S, and U optical bands. The critical challenge for MBT implementation is the availability of efficient optical amplifiers beyond the currently used C-band to extend operation of optical networks to the O-, E-, S-, and U-bands.

There have been recent significant advances in the development of various doped-fiber amplifiers [4,5], Raman amplifiers [6], fiber optical parametric amplifiers [7], and semiconductor optical amplifiers [8] operating in different telecommunication bands from the O- to U-bands. One of the promising approaches that allows signal amplification in the O-, E-, S-, and U-bands of the optical window is with the bismuth-doped fiber amplifier (BDFA) [4,9–11]. Such spectral flexibility of the BDFA is provided by different co-dopants that can be used to form different Bi-related active centers in the core of the fiber. Phosphosilicate glass shifts the gain to the O-band [4,10], silicate glass with low concentration of germanium features gain in the E- and S-bands [9], and germanosilicate fibers make it possible to achieve amplification in the U-band [11]. Despite these advances, there have been yet few demonstrations of coherent transmission using BDFAs [12]. Moreover, previously reported transmission experiments in the E-band were realized with relatively short fiber lengths [12,13].

Here we report a transmission of five widely spaced 30-GBaud dual polarization (DP) 16-QAM signals (including 4 "dummy" channels and 1 signal carrier) over a record transmission distance of 160 km using standard single-mode fiber (SSMF) in the E-band fully supported by three BDFAs. The amplifiers feature a maximum gain of 27.3 dB, 33.8 dB, and 28.3 dB, and a minimal noise figure (NF) of 4.8 dB, 4.7 dB, and 5.3 dB, respectively. The transmission performance is characterized in terms of the Q^2 factor [14] in the spectral range of 1410–1460 nm. The main factors influencing the performance of the setup are addressed and discussed.

Experimental setup. The experimental setup for the five channel DP 30-Gbaud 16-QAM transmission through a 160-km SSMF is presented in Fig. 1(a). The coarse wavelength division multiplexer (WDM) grid consists of 4 "dummy" channels at 1411 nm, 1431 nm, 1451 nm, and 1470 nm. (Note: the number of channels was limited by component availability rather than the fundamental BFDA design, i.e., there is no wavelength selective switch for channelization of a wideband source in the E-band, and there is a very limited selection of CW lasers in the E-band that can further increase the number of transmitted channels.) The data carrier signal is generated using a tuneable laser (TL) operating from 1410 to 1460 nm, which is modulated by a dual-polarization IQ modulator (DP IQ Mod) driven by a digital-to-analog converter (DAC) to achieve DP 30-GBaud 16-QAM modulation. The signal after the modulator is amplified by the booster amplifier. For power equalization of the data channel with the "dummy" channels, a variable optical attenuator

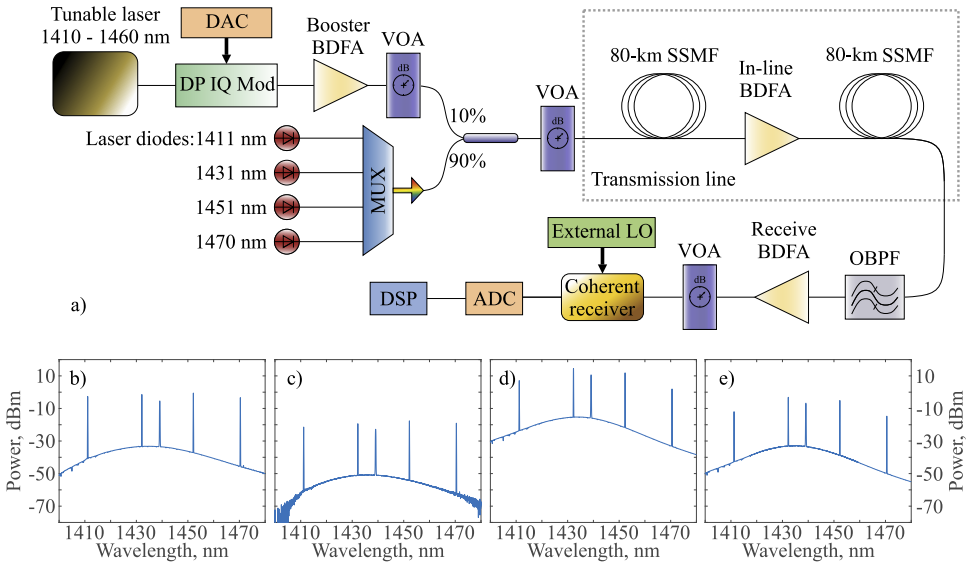

Fig. 1. (a) Experimental setup for five-channel DP 30-Gbaud 16-QAM transmission through a 160-km SSMF in the E-band; spectra of the channels (b) at the input to the transmission line, (c) after the 80-km-long SSMF, (d) after the in-line amplifier, (e) at the output of the transmission line.

(VOA) is used ahead of a 90/10 coupler. In the case of back-to-back (B2B) transmission, the signal then is directed to an optical bandpass filter (OBPF), where the data carrier is filtered. When the 160-km transmission is performed, the signal is directed into another VOA that is used to control total input power to the transmission line. Then the signal is transmitted through a 80-km-long SSMF, then amplified by the developed in-line BDFA, and transmitted through another 80-km-long SSMF. In both cases, after the data carrier is filtered by an OBPF, and it is amplified by the receive amplifier. The input power to the coherent receiver is controlled by another VOA, and an external TL operating at 1410–1460 nm is used as a local oscillator (LO) for the coherent detection system. Channel reception is completed by a standard set of 80-GSa/s, 36-GHz analog-to-digital converters (ADCs). The digital signal processing (DSP) chain used for analysis of the received signal has been described previously [15].

The spectra of the channels at different parts of the transmission line are presented in Figs. 1(b)–1(e). Figure 1(b) shows signals at the input to the transmission line. All channels have equal power per channel even though the signal at 1440 nm is a data carrier and it has a lower power spectral density due to the higher bandwidth. Figure 1(c) shows the signal after transmission through an 80-km-long SSMF. The passive loss of the SSMF is higher at lower wavelengths, which leads to the development of a tilt in the spectrum. The amplified signal after the in-line BDFA is presented in Fig. 1(d). The amplified signal is transmitted through another 80-km-long SSMF and the signal spectrum at the output of the transmission line is shown in Fig. 1,e.

The schematic depiction of the developed amplifiers is presented in Fig. 2. All of the amplifiers were optimized in terms of the best performance of the gain and NF using different pump diode wavelengths. Eachamplifier consists of an active Bi-doped fiber, two isolators for unidirectional propagation of the signal, and two thin-film-filter wavelength division multiplexers (TFF-WDMs) for multiplexing signal and pump radiation. A set of pump diodes is used for each amplifier to allow the best

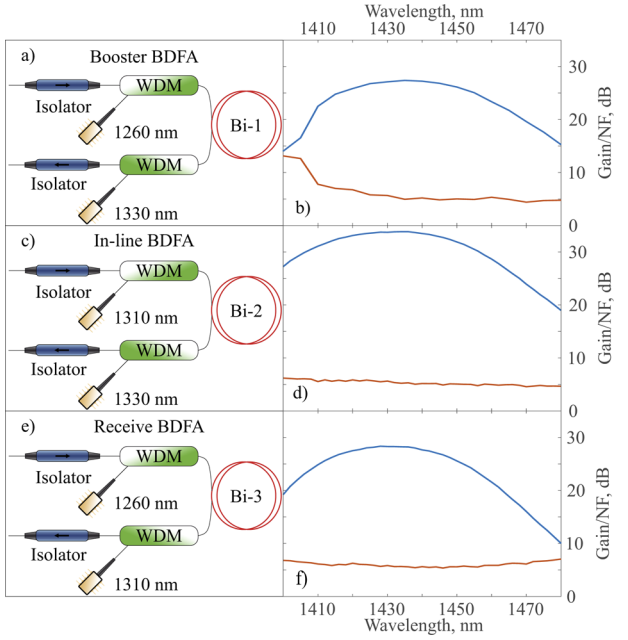

Fig. 2. Schematic of (a) booster BDFA, (c) in-line BDFA, and (e) receive BDFA; gain and NF dependencies on the wavelength of (b) booster BDFA, (d) in-line BDFA, and (f) receive BDFA.

performance in terms of gain and NF. The booster BDFA is presented in Fig. 2(a). It is based on a 153-m-long piece of germanosilicate Bi-doped fiber with the following characteristics: 6-μm fiber core diameter and a cutoff wavelength at Ĩ μm. The 1260-nm (forward) and 1330-nm pump (backward) enable a 4.8-dB NF, 27.3-dB gain, and 46-nm 3-dB bandwidth in the setup. The maximum total pump power is 900 mW for all three amplifiers. The gain and NF of the booster BDFA are presented in Fig. 2(b).

The in-line amplifier has the same schematic as the booster amplifier, however, it is based on 1310-nm (forward) and

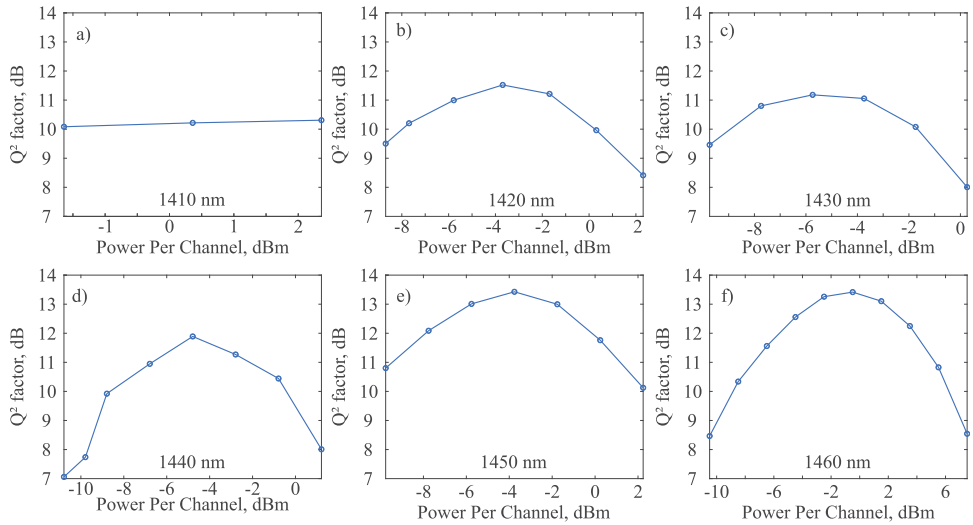

Fig. 3. Dependencies of the Q^2 factor of the transmitted signal on the input power per channel at: (a) 1410 nm; (b) 1420 nm; (c) 1430 nm; (d) 1440 nm; (e) 1450 nm; and (f) 1460 nm.

1330-nm (backward) pump diodes with total 900-mW pump power. These diodes allow bi-directional pumping of the fiber. The Bi-doped fiber is manufactured to have the same geometric characteristics as the fiber of the booster; however, it is made of a different preform with a higher bismuth concentration and has a length of 173 m. This amplifier has a maximum gain of 33.8 dB and decreased NF of 4.7 dB in comparison to the booster BDFA. The wavelength dependencies of the gain and NF for in-line BDFA are presented in Fig. 2(d). Moreover, the 3-dB bandwidth of the amplifier is 50 nm.

The schematic of the receive amplifier is presented in Fig. 2(e). The 300-m-long fiber of this amplifier was presented in [9] and has the following characteristics: the fiber core is 9 μm, and the cutoff wavelength is approximately 1.2 μm. The 1260-nm pump diode is used for forward pumping and the 1310-nm pump diode is used for backward pumping. The amplifier has a maximum gain of 28.3 dB, minimal NF of 5.3 dB, and 42-nm 3-dB bandwidth. The wavelength dependence of both gain and NF are presented in Fig. 2(f).

Results. To perform the measurements across the selected spectral interval, the operation wavelength of the input TL and the external LO TL are appropriately controlled. In this work, we experimentally characterize six wavelengths: 1410; 1420; 1430; 1440; 1450; and 1460 nm. After the wavelength is tuned, as the first step, B2B performance is recorded. The dependence of the Q^2 factor on wavelength for the B2B case is presented in Fig. 4(a) (blue line with circles). After measurements of the B2B performance, the transmission line is assembled. The power at the input to the transmission line is changed with a VOA to allow study of the performance at different per channel input powers. The dependence of the Q^2 factor on the input power per channel for all six wavelengths under test are shown in Fig. 3.

Generally, the change of the Q^2 factor with the input power per channel follows the following pattern: the Q^2 factor grows with an increase of input power per channel until an optimal point (the input power per channel with the highest Q^2 factor); after the optimal point, the Q^2 factor decreases with the increase of the input power per channel due to the nonlinear effects that lead to nonlinear signal distortions. Due to the power limitations, the Q^2 factor dependence on the input power per channel at 1410 nm is only recorded within the linear regime before an optimal point. All measurements (except one at 1410 nm) are performed in a way to determine an optimal input power per channel. The power per channel is calculated from the recorded spectra and power meter measurement at the input to the transmission line. Spectra are used to calculate a portion of the input power dedicated to the data carrier channel. It is approximately −4 dBm for 1420 nm, then it decreases up to −6 dBm for 1430 nm, then it goes up to −5 dBm, −4 dBm, and 0 dBm for 1440 nm, 1450 nm, and 1460 nm. Such a substantial variation of the optimal input power per channel for all the wavelengths can be due to several factors: non flat gain of the amplifiers, NF variations in the amplification spectra, increased loss, and decreased nonlinearity of the SSMF on the left-hand side of the spectra.

As the next step, the B2B performance of the setup to transmission are compared. The dependence of the Q^2 factor for the optimal input power per channel on the wavelength is presented in Fig. 4(a) (orange line with squares). The difference between the B2B and transmission performance is presented as a Q^2 factor penalty in Fig. 4(b). Both B2B and transmission performance rise with the increase of wavelength of the signal. This can be mostly explained by the fact that a C–L optical transceiver and receiver have been used in this work. The problem of performance degradation of C+L equipment in the S-band and beyond has been addressed in the following work [16]. Mostly, such degradation can be explained by the I/Q imbalance of the optical transceiver and polarization imbalance of the optical hybrid used in the experiment. The polarization imbalance (difference between average X and Y Q^2 factor values at each wavelength) was recorded in terms of the Q^2 factor penalty between X and Y components and is presented in Fig. 4(c). There is a significant increase of the impairment at the 1410-nm signal wavelength. This can be explained by limitations of the used optical hybrid optimized for operation in C+L bands. Generally, measurement of the pre-forward-error-correction (FEC) bit error rate (BER) is enough to predict the post-FEC BER. The 2.7×10^{-2} BER corresponding to a 5.7-dB Q^2 factor is achieved for all powers and wavelengths in the experiment. This BER has been shown to be corrected to 10^{-15} and below using soft-decision FEC with 20% overhead [17].

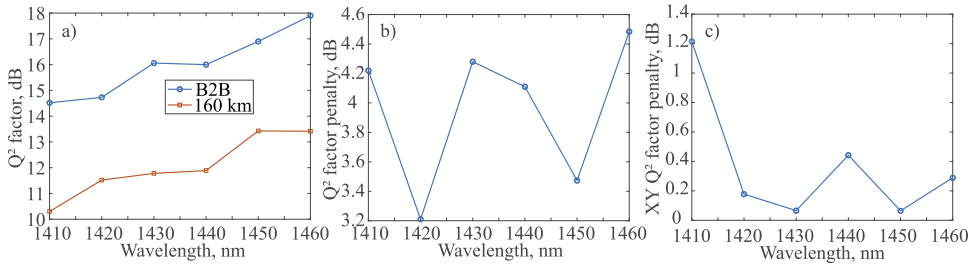

Fig. 4. (a) Spectral dependence of the Q^2 factor for the B2B case (blue line with circles) and transmitted signal (orange line with squares); (b) spectral variation of the Q^2 factor penalty between the B2B and transmitted signal cases; (c) dependence of the polarization Q^2 factor penalty on wavelength.

Finally, it is important to discuss the results of the Q^2 factor penalty in the E-band. The maximum penalty is 4.5 dB at 1460 nm and the lowest penalty is 3.2 dB at 1420 nm. There is no clear tendency of the Q^2 factor penalty dependence on wavelength in the E-band due to complexity of the system and number of factors that impact the performance of the setup. However, it is insightful to address the impacts of various factors at different wavelengths. First of all, the shorter wavelength region features high optical loss, relatively low gain, high NF, and the increased polarization or I/Q imbalance. Longer wavelengths suffer from both increased dispersion and low gain. However, transmission in this region benefit from lower loss and NF, and lower transceiver–receiver-induced penalties. However, the nonlinearity can be the dominating factor at wavelengths 1430–1440 nm due to increased gain in this region. The use of a gain-flattening filters can potentially improve the performance of the transmission line by significantly decreasing the nonlinearity in the 1430–1440-nm range. However, the BDFAs should potentially be improved more in terms of NF at the lower wavelengths (<1430 nm).

Conclusion. To conclude, we have demonstrated the transmission of five 30-GBaud DP 16-QAM signals (coarsely spaced) over 160-km in the spectral E-band (1410–1460 nm). This is, to the best our knowledge, the record transmission length for this spectral band. The experimental setup was based on C+L compatible receiver and transmitter components and in-house BDFAs for booster, in-line, and receive amplification. The system penalties were analyzed and the main factors leading to them were highlighted. The performance of the system was well above the pre-FEC soft decision threshold for 10^{-15} post-FEC BER. The achieved performance indicate that the BDFA is a promising solution for expanding current optical telecommunication bandwidth beyond C+L bands toward the E-band.

Funding. HORIZON EUROPE Marie Sklodowska-Curie Actions (813144, 814276); Engineering and Physical Sciences Research Council (EP/R035342/1, EP/S003436/1, EP/S016171/1, EP/V000969/1).

Acknowledgments. The authors are grateful to Dr. V.M. Mashinsky and Dr. M. Melkumov from FORC, Moscow, Russia, for provision of the Bi-doped fibers.

Disclosures. The authors declare no conflicts of interest.

Data availability. Data underlying the results presented in this paper are not publicly available at this time but may be obtained from the authors upon reasonable request.

REFERENCES

1. P. J. Winzer, D. T. Neilson, and A. R. Chraplyvy, Opt. Express **26**, 24190 (2018).
2. A. Ferrari, A. Napoli, J. K. Fischer, N. M. S. Da Costa, A. D'amico, J. Pedro, W. Forysiak, E. Pincemin, A. Lord, A. Stavdas, J. P. Fernandez-palacios Gimenez, G. Roelkens, N. Calabretta, S. Abrate, B. Sommerkorn-krombholz, and V. Curri, J. Lightwave Technol. **38**, 4279 (2020).
3. A. D. Ellis, J. Zhao, and D. Cotter, J. Lightwave Technol. **28**, 423 (2010).
4. Y. Ososkov, A. Khegai, S. Firstov, K. Riumkin, S. Alyshev, A. Kharakhordin, A. Lobanov, A. Guryanov, and M. Melkumov, Opt. Express **29**, 44138 (2021).
5. J. W. Dawson, L. S. Kiani, P. H. Pax, G. S. Allen, D. R. Drachenberg, V. V. Khitrov, D. Chen, N. Schenkel, M. J. Cook, R. P. Crist, and M. J. Messerly, Opt. Express **25**, 6524 (2017).
6. M. Tan, P. Rosa, S. Le, M. A. Iqbal, I. Phillips, and P. Harper, Opt. Express **24**, 2215 (2016).
7. C. B. Gaur, V. Gordienko, F. Bessin, and N. J. Doran, in *in 2020 European Conference on Optical Communications (ECOC)* (IEEE, 2020), pp. 1–4.
8. J. Renaudier, A. Arnould, A. Ghazisaeidi, D. Le Gac, P. Brindel, E. Awwad, M. Makhsiyan, K. Mekhazni, F. Blache, A. Boutin, L. Letteron, Y. Frignac, N. Fontaine, D. Neilson, and M. Achouche, J. Lightwave Technol. **38**, 1071 (2020).
9. A. Donodin, V. Dvoyrin, E. Manuylovich, L. Krzczanowicz, W. Forysiak, M. Melkumov, V. Mashinsky, and S. Turitsyn, Opt. Mater. Express **11**, 127 (2021).
10. N. Thipparapu, Y. Wang, A. Umnikov, P. Barua, D. Richardson, and J. Sahu, Opt. Lett. **44**, 2248 (2019).
11. S. Firstov, K. Riumkin, A. Khegai, S. Alyshev, M. Melkumov, V. Khopin, F. Afanasiev, A. Guryanov, and E. Dianov, Laser Phys. Lett. **14**, 110001 (2017).
12. A. Donodin, M. Tan, I. Phillips, A. A. Ali, P. Hazarika, M. Patel, P. Harper, V. Dvoyrin, W. Forysiak, and S. Turitsyn, in *Optical Fiber Communication Conference* (Optica Publishing Group, 2022), pp. W3J–S5.
13. S. Okamoto, K. Minoguchi, F. Hamaoka, K. Horikoshi, A. Matsushita, M. Nakamura, E. Yamazaki, and Y. Kisaka, J. Lightwave Technol. **38**, 1061 (2020).
14. A. Ellis, M. McCarthy, M. Al Khateeb, M. Sorokina, and N. Doran, Adv. Opt. Photonics **9**, 429 (2017).
15. P. Skvortcov, I. Phillips, W. Forysiak, T. Koike-Akino, K. Kojima, K. Parsons, and D. S. Millar, IEEE Photonics Technol. Lett. **32**, 967 (2020).
16. R. Emmerich, M. Sena, R. Elschner, C. Schmidt-Langhorst, I. Sackey, C. Schubert, and R. Freund, J. Lightwave Technol. **40**, 1360 (2022).
17. D. Chang, F. Yu, Z. Xiao, N. Stojanovic, F. N. Hauske, Y. Cai, C. Xie, L. Li, X. Xu, and Q. Xiong, in *OFC/NFOEC* (IEEE, 2012), pp. 1–3.